JOURNAL OF PROPULSION AND POWER
Vol. 21, No. 1, January–February 2005

Acoustic Detection of Blowout in Premixed Flames

Suraj Nair* and Tim Lieuwen†
Georgia Institute of Technology, Atlanta, Georgia 30332-0150

Work to develop a practical, fast diagnostic technique to monitor the proximity of a combustor to blowout using measurements of the flame's acoustic signature is described. The feasibility of this approach was demonstrated on three combustors with different flame holding mechanisms that are used in most practical combustion devices: pilot, swirl, and bluff-body stabilized flames. Extensive high-speed flame images were obtained and analyzed in conjunction with simultaneous acoustic data. These analyses revealed changes in the low-frequency spectrum and/or the increased presence of time-localized and intermittent events in the acoustic data as the combustor approached blowout. Based on these observations, spectral, statistical, wavelet, and thresholding signal-processing schemes were developed for detecting blowout precursors with varying levels of time response, sensitivity, and robustness.

I. Introduction

PRACTICAL combustors are required to operate over a wide range of operating conditions with high levels of combustion efficiency. However, blowout is a serious concern in modern, highly loaded land-based and aeroengine combustors, particularly in aircraft engines where the combustion process is ultimately the source of the vehicle's thrust. It is a particular concern in both military and commercial aircraft during sudden changes in throttle setting. For example, during rapid decelerations, the fuel flow rate can be reduced very quickly, whereas the slower airflow transient rate is controlled by the rotational inertia of the compressor.[1] When coupled with overall engine system dynamics, flame blowout can result in the inability of an engine to recover from a compressor stall event.[2] Blowout is particularly dangerous in high-altitude vehicles where the stability limits are narrowed, which may necessitate their descent to lower altitudes to relight.

Blowout is also a major concern in land-based, industrial systems, where the engines are required to operate economically and reliably over long periods with minimal shutdown time. Emissions legislation has motivated the design of lean, premixed combustors that operate near the blowout limit. Under these lean conditions, the combustion process is vulnerable to small perturbations in combustor conditions, particularly during load changes or because of changes in fuel composition[3] or air temperature and humidity. In land-based gas turbines, such blowout events may require a lengthy (and therefore expensive) system shutdown and restart, which increases maintenance costs and reduces engine life and availability.

Currently, blowout is avoided by the operation of the combustor with a wide margin from the somewhat uncertain stability limit. Precise, real-time knowledge of this margin would allow it to be reduced, resulting in lower pollutant emissions and enabling faster engine transients. The ability to sense blowout precursors can, therefore, provide significant payoffs in engine reliability and operability, in enabling optimal performance over extended time periods as an engine ages, in reducing maintenance costs, and in increasing engine life. The objective of this work is to develop a practical diagnostic that can sense the proximity of the combustor to blowout and be incorporated into a blowout prevention or control scheme.

Presented as Paper 2003-5084 at the AIAA 39th Joint Propulsion Conference, Huntsville, AL, 20–23 July 2003; received 7 October 2003; revision received 9 September 2004; accepted for publication 13 September 2004.

*Graduate Research Assistant, School of Aerospace Engineering, 635 Strong Street; gt6110b@acme.gatech.edu. Student Member AIAA.

†Assistant Professor, School of Aerospace Engineering, 270 Ferst Drive; tim.lieuwen@aerospace.gatech.edu. Member AIAA.

II. Background

The parameter space over which sustained combustion occurs in practical combustors is sometimes referred to as the region of static stability of the combustion process. The loss of static stability is referred to as blowout. The term static stability is used to distinguish blowout from dynamic stability, which usually refers to self-excited, combustion-driven oscillations that involve chemical energy being fed into acoustic oscillations.[4,5]

A stable flame can be sustained in the combustor only over a certain range of fuel/air ratios.[6] Several studies have observed enhanced unsteadiness in the flame characteristics when a flame is near blowout, but is statically stable, or when an operating condition is changed such that the combustor moves from stable combustion to blowout. These observations are the basis for the work described here. For example, Nicholson and Field[7] observed large-scale, irregular pulsations of a bluff-body stabilized flame as it was blowing off. They reported that the main flame periodically detached and reattached to the flame holder before it became completely extinguished. Note that this unsteadiness was not observed after the fact, that is, after the flame had blown off and was convecting out of the combustor. Rather, the flame was still observed behind the bluff body during these pulsations. More recently, Chao et al.[8] characterized a turbulent nonpremixed jet flame during the blowout process. They reported that before blowout, the flame base pulsated from attachment to nonattachment at the burner lip. They found that this regime could persist over time intervals from a few pulsation cycles to several seconds.

A significant amount of early work was performed to understand the mechanisms of flame stabilization in bluff-body,[9–13] swirl,[14] dump, and pilot[10] stabilized flames in high-velocity streams. However, the focus of this literature is primarily devoted to the prediction of the blowout limits of a given system as a function of such parameters as equivalence ratio, air temperature, or pressure. With the exception of the work of Chao et al.,[8] little has been done to characterize the combustion processes as it transitions from static stability to blowout. The objective of the present work is to characterize the acoustic emissions of premixed flames under such circumstances. This objective is motivated by the desire to develop practical, fast diagnostic techniques that can be used to detect the onset of blowout.

Acoustic emissions provide a useful diagnostic into transient flame holding events because they are proportional to the temporal rate of change of heat release.[15] Furthermore, many land-based systems are already instrumented with dynamic pressure transducers. As such, implemention of the developed precursor detection technique simply requires insertion of a software module into the existing monitoring software.

Combustion noise is generated fundamentally by the unsteady expansion of reacting gases. It is known that the acoustic emissions of turbulent flames are dominated by unsteady heat release processes (as opposed to flow noise)[16] that excite acoustic waves over a broad range of frequencies (typically, between ∼10 Hz and 25 kHz). Thus, acoustic measurements can be used to detect either global changes in heat release rate or fluctuations in heat release at certain timescales by measurement of their acoustic emissions in corresponding frequency bands.

In the majority of combustors, the flame is stabilized either by an external pilot flame (or some other persistent source of heat and/or fuel radicals) or fluid mechanic recirculation of hot products, such as in swirl-stabilized systems or in the wake behind a bluff body. This paper presents measurements taken from premixed flames in atmospheric-pressure combustors with the three aforementioned flame holding mechanisms. The following section describes the experimental setup, instrumentation, and data reduction schemes. Then we present typical results and discuss the phenomenology of the acoustic radiation encountered near blowout.

III. Experimental Facility and Instrumentation

A. Piloted Burner

A schematic of the piloted, natural gas fueled, 50-kW burner used in this study is shown in Fig. 1. The burner tube is 110 mm long and was sized to ensure fully developed pipe flow at its exit. The main burner consists of a 23-mm stainless steel tube and is surrounded by a circumferential array of 24 × 1.6 mm diameter pilot holes. The fuel and airflow rates into the main and pilot burner were controlled separately. The pilot flames anchor the main flame at high flow velocities. The flow control and monitoring system have a resolution of approximately 0.01 in equivalence ratio ϕ. The flow rates were measured with rotameters for all of the burner configurations.

B. Swirl Stabilized Burner

A schematic of the 100-kW, swirl-stabilized combustor is shown in Fig. 2. A premixed methane–air mixture passes through swirl vanes housed in a 23-mm tube. The exit of the jet has a swirler with vane angle of 30 deg, which is equivalent to a swirl number of approximately 0.39 (Ref. 17). The flow expands into a cylindrical 70-mm-diam and 190-mm-long combustion chamber. The combustor wall provides confinement to the flow and is responsible for generating a recirculating outer flow that helps stabilize the flame at high velocities. The combustor walls are quartz to facilitate flame visualization. The flow control and monitoring system have a resolution of approximately 0.003 in equivalence ratio ϕ. All measurements were made at atmospheric conditions.

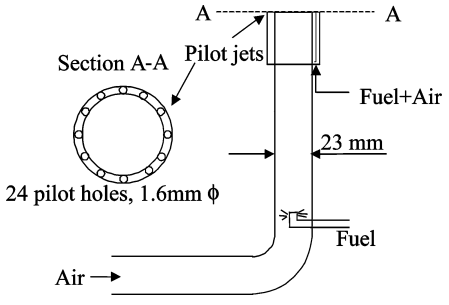

Fig. 1 Schematic of 50-kW ring-piloted burner.

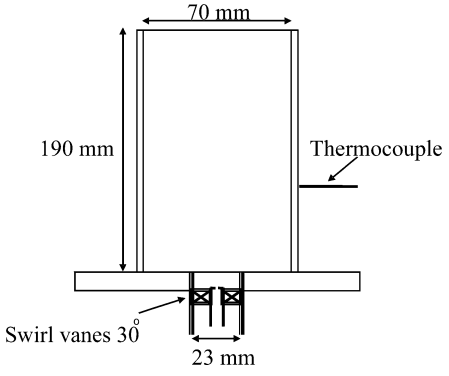

Fig. 2 Schematic of 100-kW swirl combustor.

C. Bluff-Body Stabilized Burner

The piloted burner shown in Fig. 1 was also used for bluff-body stabilized flame studies. Bluff bodies of various cross sections and diameters were placed above the burner exit and secured by posts anchored at the burner exit flange. Results presented here are for a cylindrical rod with a 1 cm diameter at a standoff height of 5 cm from the burner exit.

D. Instrumentation

Acoustic oscillations were measured with calibrated, Bruel and Kjaer type 4191 condenser microphones that have a flat frequency response up to 40 kHz. The microphones were located ∼61 cm from the combustor exit at ∼30 deg from the flow axis for all of the burners. We found that the flame noise exhibited little directivity, and, thus, the results demonstrated little dependence on microphone location. The principal exception to this is if the microphone is placed in the combustion exhaust or entrainment flow. In this case, hydrodynamic pressure fluctuations substantially increase background noise levels. The microphone output was low-pass filtered at 1 kHz and then fed into a 12-bit National Instruments A/D board. (Analysis of acoustic data at frequencies higher than 1 kHz did not reveal additional information that could be used for blowout detection.) A total of 65,536, that is, 2^{16}, data points were obtained at each operating condition with a sampling frequency of 2 kHz. High-speed images of the flame under stable and near blowout conditions were obtained to better understand the phenomenology of the flame blowoff process and, hence, to improve capabilities for interpretion of the acoustic signature. The high-speed bluff-body flame images shown in the next section were obtained with a charge-coupled device camera (Red Lake Motionscope 280 × 320 full frame resolution) at 500 frames/s with a shutter speed of 1 ms.

Simultaneous chemiluminescence measurements were also obtained in the swirl combustor. A lens-based collection setup consisting of a 25-mm-diam, 25-cm focal length lens was used to collect the light from the combustor and image it onto a photo-multiplier tube [(PMT) Hamamatsu R928] through an aperture. The PMT operates with a supply voltage of 900 V and a 10-kΩ external load resistor, which produce an effective bandwidth of 200 kHz. This optical path also includes an interference filter centered at 308 nm (20-nm full-width-half-maximum), corresponding to the OH electronic transition. In addition, a neutral density filter with optical density of 1.0 was used to reduce the intensity of light collected and to prevent saturation of the chemiluminescence signal.

Exhaust emissions were measured with a Lancom Portable Gas Analyzer sampled through a 30-cm probe with a sintered filter. The analyzer calibration was checked with bottled calibration gases before and after each test sequence.

IV. Blowout Phenomenology

A. Piloted Burner

In this section, we describe the phenomenology of the flame blowout process. For the piloted burner, data were obtained under several operating conditions where both the main and pilot fuel and airflow rates were varied. The velocity in the main flow was maintained at high values (>15 m/s), so that the flame could only be stabilized with the pilots on. (Without the pilot, the main flame can only be anchored for velocities below ∼1 m/s.) The flame's proximity to blowout was controlled via the flow rate of fuel to the pilot, which was operated fuel rich. Representative data shown here were acquired at an equivalence ratio of $\phi = 0.88$, average cold flow velocity of $u = 16$ m/s, and piloting fuel fraction ranging from 5 to <1%, where the equivalence ratio of the pilot flame varied between 0.7 and 1.3. Under stable conditions, the flame is firmly anchored

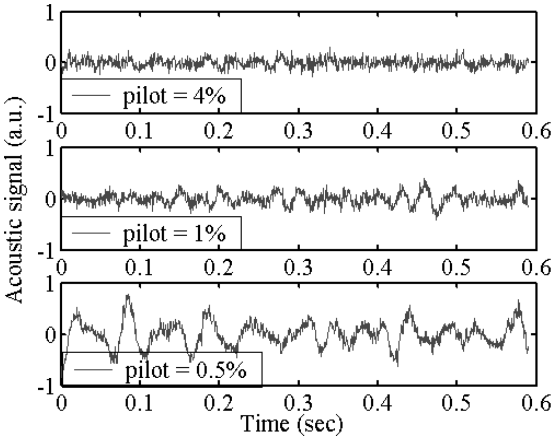

Fig. 3 Acoustic signatures from piloted burner for piloting percentages of 4.0, 1.0, and 0.5% at $\phi = 0.88$.

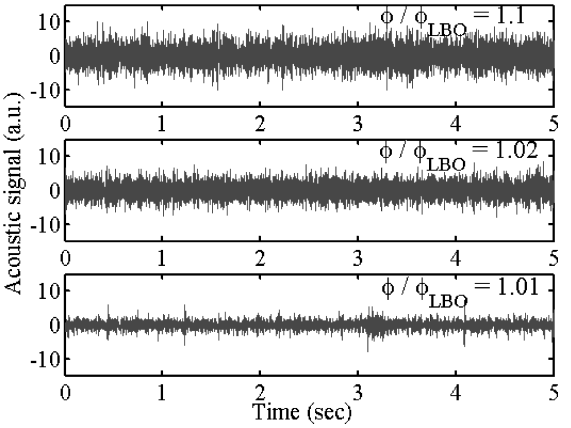

Fig. 4 Acoustic signal from swirl burner for $\phi/\phi_{LBO} = 1.1$, 1.02, and 1.01.

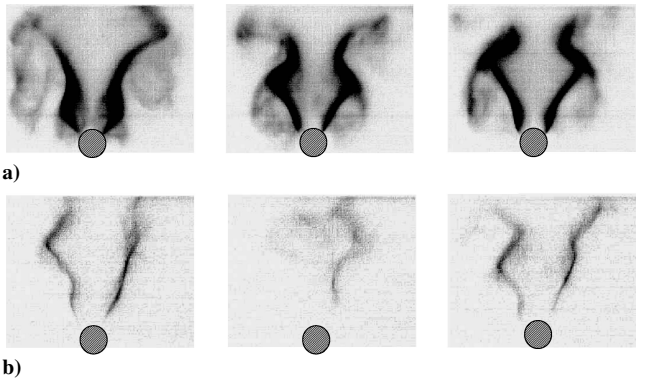

Fig. 5 High-speed camera images of a) stable combustion mode at $\phi/\phi_{LBO} = 1.4$ and b) close to blowout at a $\phi/\phi_{LBO} = 1.1$; $u = 9.8$ m/s for bluff-body burner.

by the pilot flames. As the pilot fuel is turned down and blowout is approached, the flame no longer symmetrically attaches around the edge of the burner. Instead, it periodically detaches from one side of the burner, remains anchored by several pilot holes, and then reverts back to its symmetric stabilization. This phenomenon of detachment and reattachment increases in frequency and duration as the blowout point is approached. Very near the blowout point, the flame anchors only onto a few points and does not exhibit this unsteady detachment/reattachment behavior. When the flame is not uniformly attached very near blowoff, the tip region flaps radially back and forth more violently than it does when it is well stabilized. This is apparently the reason for the presence of enhanced low-frequency acoustic emissions near blowout, as shown in Fig. 3. Figure 3 shows typical time dependencies of the combustion noise measured from the piloted burner as it approaches blowout.

Approximate CO measurements were also taken at the burner centerline, 2 cm above the flame tip, to determine the dependence of combustion efficiency on piloting level. Although not shown, these measurements indicate that the uncorrected CO levels increased from 9 ppm in the well-anchored flame to ~20 ppm before blowout.

B. Swirl Burner

The swirl burner's proximity to blowout was controlled by the equivalence ratio, which was adjusted via the overall fuel flow rate, whereas the overall airflow was kept fixed. The data presented here correspond to a bulk average velocity of 6.6 m/s at the combustor exit under cold, atmospheric conditions. The overall equivalence ratio was varied between 0.7 and 1.1. The blowout equivalence ratio for this combustor is just below 0.75 for the flow conditions used. Near blowout, the flame was very unsteady. High-speed movies revealed the presence of near total flame extinction followed by reignition. The occurrence and duration of these events (which span a few milliseconds) increases as the flame approaches lean blowout (LBO),[18] as will be discussed later.

Figure 4 shows typical measured time dependencies of the acoustic pressure at several normalized equivalence ratios, $\phi/\phi_{LBO} = 1.1$, 1.02, and 1.01. Note the reduction in rms pressure levels with equivalence ratio, apparently due to the reduced heat release rates[15] at the lower fuel flow rates. Near blowout, short time duration, high-amplitude bursts are observed. Comparison of these time series with corresponding OH^* chemiluminescence signatures indicated that these bursts coincided with the occurrence of the flame loss and reignition events described earlier.

CO emission measurements were also taken at the combustor exhaust to determine the dependence of combustion efficiency on ϕ/ϕ_{LBO}. Although not shown, CO levels increased from ~75 to 350 ppm under stable and near blowout conditions, respectively. This increase is largely due to the lengthening of the combustion zone to the point where it extends past the emissions probe.

C. Bluff-Body Burner

Representative data presented here correspond to a bulk average velocity of 9.8 m/s at the burner exit under atmospheric conditions. The flame's proximity to blowout was controlled via the overall fuel flow rate, where the blowout equivalence ratio was 0.9. Figure 5a shows several direct images (no spectral filter) of a stable flame at $\phi/\phi_{LBO} = 1.4$, that is, far from blowout. In Fig. 5a, the symmetric, counterrotating vortices shed behind the flame holder are evident, similar to previous observations.[19] Figure 5b shows the flame behavior near blowout. Close to blowout, the reaction zone is visibly weaker and the flame wrinkles no longer have the symmetric structure. In some cases, one of the flame branches is apparently almost extinguished, nearly disappearing from the field of view. This is followed by the reemergence of the flame, suggesting reignition of unburnt fuel in the shear layer. There is periodic detachment and reattachment of the weak flame to the flameholder. The occurrence of these partial extinction and reignition events (spanning 40–80 ms) increases as the flame approaches lean blowout. Although not shown, the rms pressure levels monotonically decrease with equivalence ratio, as was also observed in the swirl burner.

V. Acoustic Signal Analysis

A. Signal Analysis Strategies

Developing data analysis schemes with maximum sensitivity, speed, and robustness requires an understanding of the flame characteristics preceding blowout. The high-speed flame images obtained in conjunction with simultaneous acoustic data were used to aid the development of such strategies. These analyses revealed that as the flame approached blowout, the average spectral characteristics of its acoustic emissions changed, particularly in the pilot flame. In addition, increases in number and duration of time-localized bursts (events) in the signal were often observed in the swirl and

bluff-body burners. Based on these observations, three basic signal-processing methods were evaluated for the extraction of blowout precursors: conventional spectral or wavelet-based time–frequency analysis, statistical analysis, and threshold-crossing analysis. Conventional power spectra were estimated from averages of 32 ensembles. The primary limitation of this approach is its insensitivity to time-localized events. This shortcoming can be circumvented to some extent (within the limitations of the time–frequency uncertainty principle[20]) with time-frequency data analysis performed with the wavelet transform. The wavelet transform is defined as

$$f_\psi(t) = \int_{t'} W[(t'-t)/\psi]p(t')\,\mathrm{d}t' \tag{1}$$

where $p(t)$ is the raw time series data, ψ is a scaling parameter, and $W(t)$ is the wavelet basis function. For example, the "Mexican hat" is a popular wavelet whose functional dependence is given by

$$W_1(t) = \left(2/\sqrt{3}\right)\pi^{-\frac{1}{4}}(1-t^2)\exp(-t^2/2) \tag{2}$$

The wavelet operation is a generalization of a moving Fourier transform that is recovered when the kernel $W(t)$ is replaced by the complex exponential e^{-it}. In this case, the parameter ψ is the inverse of the frequency, $\psi = 1/f$. Its basic operation is to determine how much the pressure in some localized interval around time t looks like the wavelet basis function $W(t)$ at the scale ψ. Thus, it can be used to detect features with certain prescribed characteristics and timescales. This is useful for cases where we know a priori the temporal characteristics of the blowout precursor. By defining a wavelet with these characteristics, the wavelet operation can be used to extract such precursors from noisy data.

Statistical approaches were also used to detect changes in acoustic signal statistics. In particular, higher-order moments are sensitive to intermittent events in the signal. The nth statistical moment is defined here as

$$M_n = \left\{\frac{1}{T}\int_{t=0}^{T}[p(t)-\bar{p}]^n\,\mathrm{d}t\right\}\Big/\sigma^{n/2} \tag{3}$$

where $\bar{p}$ and σ are the pressure's time average and variance, respectively. Finally, thresholding analysis was used to detect time-localized events in the signal, such as large bursts during extinction or reignition. The basic idea behind this approach is to count the duration and/or number of times the instantaneous signal level crosses a threshold value, usually defined as some multiple of the signal's mean or variance. Because the acoustic signal is a spatially integrated measure of the unsteady heat release over the entire flame, pronounced heat release changes in a localized region of the flame may not be very evident in the overall signal. As such, we found thresholding techniques to be most useful when performed after the acoustic data are preprocessed, such as with a wavelet filter or moving average statistical moment. In contrast, because optical measurements can be focused on localized spatial regions, thresholding of the raw signal is adequate.[18]

Consider the following issues and tradeoffs associated with three key performance metrics of a blowout detection scheme:

1) Time response is a critical feature if it is to be used in systems where blowout is to be avoided during fast transients. For example, a time response of less than 1 s may be required in a high-performance military engine that must remain stable during very rapid throttle increases or decreases. A key tradeoff exists between fast time response and robustness because false alarms can be minimized and confidence in blowout proximity can be maximized by an increase in the amount of data considered in the estimation of blowout proximity.

2) The issue of sensitivity necessitates consideration of the dependence of some quantitative blowout indicator I_v, for example, the number of signal threshold crossings, on a parameter that affects the flame stability P_{FS}, (for example, equivalence ratio, pilot level or mean pressure) (see Fig. 6). First, it is critical that the ratio of I_v near blowout to when the flame is well stabilized should be very large relative to inherent noise or uncertainty, that is, $I_{v,\mathrm{blowout}}/I_{v,\mathrm{safe}} \gg 1$.

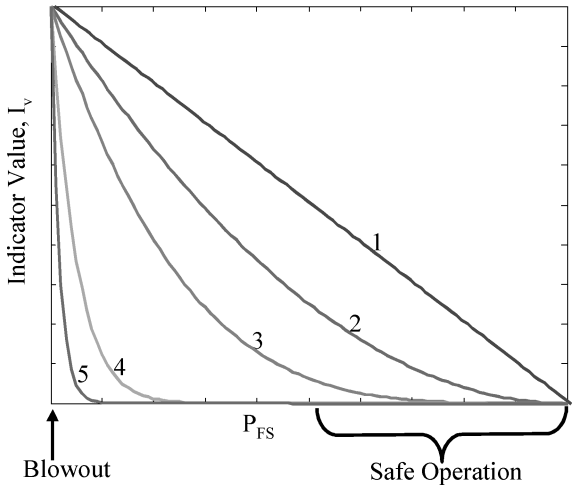

Fig. 6 Dependence of quantitative blowout indicator I_V on parameter affecting flame stability P_{FS}.

Second, the indicator value should have a one-to-one correspondence with blowout proximity. That is, it should increase monotonically as blowout is approached. All five curves shown in Fig. 6 satisfy this requirement. Third, the functional dependence of I_v on P_{FS} is important. With reference to Fig. 6, it seems preferable that the curves have a change in gradient, $\mathrm{d}I_v/\mathrm{d}P_{\mathrm{FS}}$ near blowout, such as is manifested in curves 3, 4, and 5. In contrast, the dependence of I_v on P_{FS} in curve 1 is not ideal because I_v achieves significant nonzero values even when the system is still very safe and when $\mathrm{d}I_v/\mathrm{d}P_{\mathrm{FS}}$ has a constant value that is independent of P_{FS}. Fourth, the optimal P_{FS} value where the $\mathrm{d}I_v/\mathrm{d}P_{\mathrm{FS}}$ change occurs is important. It is preferable that P_{FS} not be overly conservative and that it occurs in regions that are still quite safe, for example, curve 2. However, it should not also occur too close to the point of blowout, as in the case of curve 5.

As we will show later, the shape of the I_v vs P_{FS} curve can be manipulated to some extent through suitable changes in signal processing parameters, such as threshold levels. There is often a tradeoff in these first and fourth requirements because signal processing parameters that result in larger $I_{v,\mathrm{blowout}}/I_{v,\mathrm{safe}}$ values generally result in P_{FS} vs I_v curves resembling curves 1 or 2. In contrast, the more ideal curves 3 or 4 often have substantially lower $I_{v,\mathrm{blowout}}/I_{v,\mathrm{safe}}$ values.

3) As mentioned earlier, the signal analysis approach must also be robust to inherent levels of noise and uncertainty. Obviously, robustness of a particular approach is enhanced by the presence of a large number of ensembles of data to average out noise. In addition, I_v values at a fixed P_{FS} must be relatively insensitive to small deviations in signal processing parameters, for example, threshold level, and system aging.

B. Spectral Analysis

This section describes the Fourier analysis of the acoustic data from the three burners. Figure 7 shows the acoustic spectra from the piloted burner at three piloting levels, ranging from a well-stabilized condition (pilot fuel fraction = 5% of overall) to a point near blowout (0.6%) at a fixed equivalence ratio $\phi = 0.88$. As indicated in Fig. 7, there is a marked increase in the 10–150 Hz frequency regime under these near blowout conditions. Note also the strong peak that appears in the vicinity of 15 Hz under near blowout conditions. Data taken at several flow velocities and burner diameters also exhibited a similar peak at 15 Hz. A similar peak is faintly seen in the cold flow noise spectra and is apparently amplified in the reacting case. These data indicate that the proximity of the combustor to blowout can be monitored via acoustic power at the low-frequency bands. Figure 8 shows the dependence of the acoustic power in the 10–100 Hz and 10–20 Hz frequency range, normalized by the total power in the acoustic signal, on piloting level. Figure 8 is scaled by the minima for comparison with other burners and shows that the power

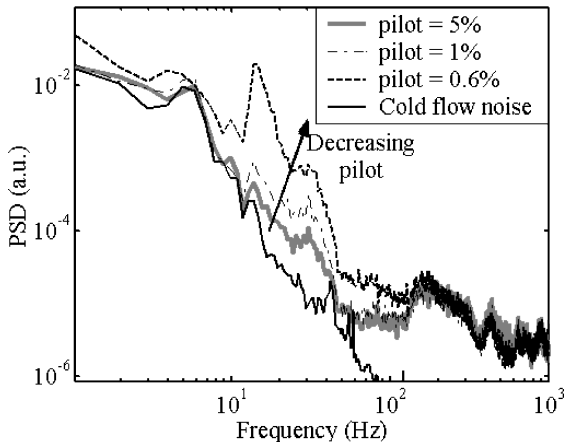

Fig. 7 Acoustic spectra of cold flow noise and combustion noise from piloted burner for piloting percentages of 5.0, 1.0, and 0.6% at $\phi = 0.88$.

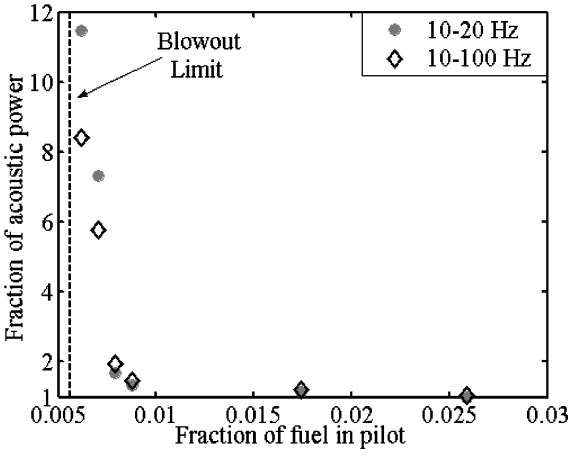

Fig. 8 Dependence of normalized acoustic power (scaled by minima) in piloted burner in 10–100 Hz and 10–20 Hz frequency bands on piloting level.

in the 10–100 Hz spectral band increases by a factor of eight as blowout is approached. Note that higher sensitivity (but slower time response) can be achieved by the examination of a similar ratio, but with a narrower bandwidth (10–20 Hz). For reference, recall that the corresponding CO emissions increased by a factor of two.

Similarly, there is a marked relative increase in low-frequency acoustic power in the swirl burner under near flameout conditions. The low-frequency increase is likely related to two timescales associated with the precursor events as observed in high-speed images. The first timescale, 10–15 ms (~100 Hz), corresponds to the no-flame duration. The second timescale is the time between such events, around 1 s or less (above a few Hertz). Results similar to those shown in Fig. 8 were also obtained here, with the power in the 10–100 Hz spectral band increasing by a factor of nearly 60 near blowout. Recall that the corresponding CO emissions increased by a factor of five.

Similar results were observed in the bluff-body burner. For example, the power in the 10–100 Hz regime increases by a factor of nearly three as blowout is approached. This can be contrasted with values of 60 and 8 for the swirl and piloted burners, respectively. Because it is an unducted burner, fuel could escape around the sides, and, hence, CO emissions were not measured.

C. Time-Frequency/Wavelet Approaches

The acoustic data from the three burners were also examined by the use of wavelet analysis as explained earlier. As alluded to in the context of Fig. 4, wavelets were found to be most useful for the swirl and bluff-body burners where time-localized events in the signal (which do not have a large impact on the average spectra) become more pronounced. In contrast, straightforward Fourier analysis is sufficient for the piloted burner (as shown in Fig. 3) where the overall average characteristics of the signal change. In contrast to the other two burners, time-localized events are less evident in the piloted burner. For this reason, we do not include any wavelet analysis of the piloted burner data, for which results similar to those shown in Fig. 8 were observed for a variety of wavelets.

To increase sensitivity, customized wavelets, which resembled the actual acoustic events close to blowout, were determined for the swirl burner. The temporal characteristics of these events were determined from simultaneous analysis of OH chemiluminescence and the acoustic signal. Figure 9a shows acoustic and optical data at an equivalence ratio close to blowout. A detail of these data is also shown in Fig. 9b. The large dips in the optical signal coincide with local temporary flame loss. A coincident feature is also evident in the acoustic signal, which resembles the derivative of the OH* signal, as expected.[15] Based on this acoustic waveform, the following customized wavelet was generated:

$$W_2(t) = -\frac{\mathrm{d}}{\mathrm{d}t}\left[\exp\left(\frac{-t^2}{2}\right)\right] \tag{4}$$

Figure 10 shows the computed $W_2(t)$ wavelet coefficients at a scale $\psi = 1/10$ s. In contrast to the overall signal variance, for example, Fig. 4, the wavelet-filtered variance actually increases as the combustor approaches blowout. In addition, large-amplitude bursts in the signal (events) are increasingly obvious. The wavelet-filtered variance of the acoustic signal increases in a similar manner to those as shown in Fig. 8. The variance increases by a factor of 60 and 40 at scales $\psi = 1/10$ s and 1/125, respectively, as blowout is approached. Also note that other wavelet basis functions give comparable results, that is, the sensitivity of the wavelet coefficient

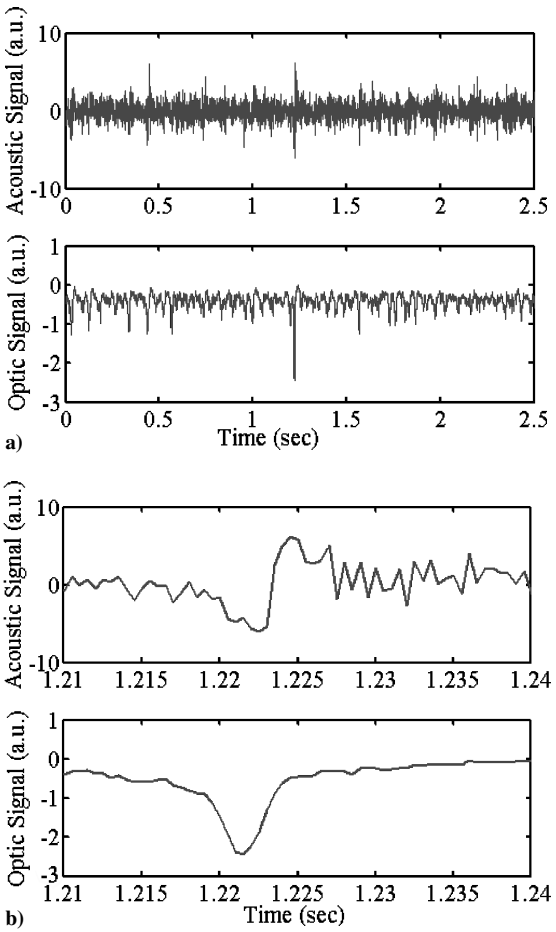

Fig. 9 Acoustic and OH* chemiluminescence time series data from swirl burner for a) $\phi/\phi_{LBO} = 1.02$, 2.5-s time segment and b) detail of blowout precursor in acoustic and optic signal.

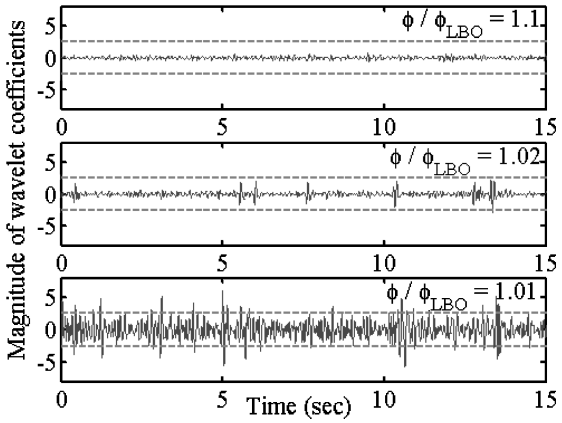

Fig. 10 Time dependence of acoustic $W_2(t)$ wavelet coefficients at $\psi = 1/10$ s for $\phi/\phi_{LBO} = 1.1$, 1.02, and 1.01 from swirl burner.

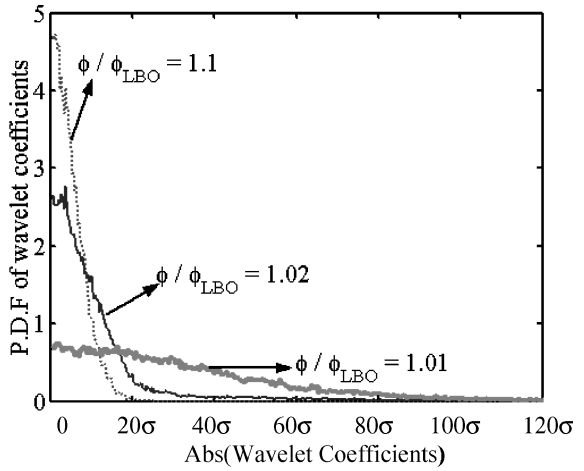

Fig. 11 Wavelet transform PDF [with $W_2(t)$] from swirl burner at $\psi = 1/10$ s for $\phi/\phi_{LBO} = 1.1$, 1.02, and 1.01.

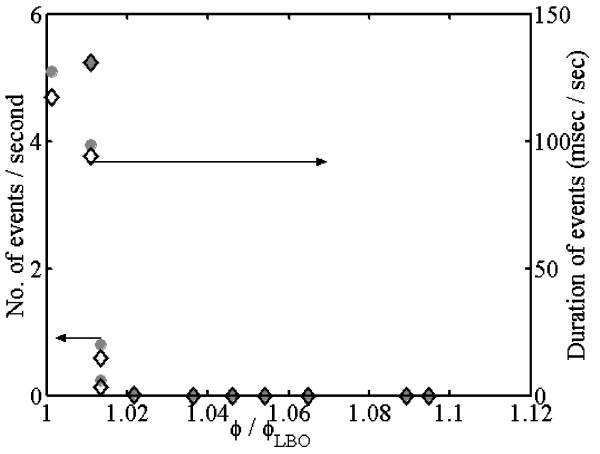

Fig. 12 In swirl burner, ●, dependence of number and ♦, duration of events on ϕ/ϕ_{LBO}.

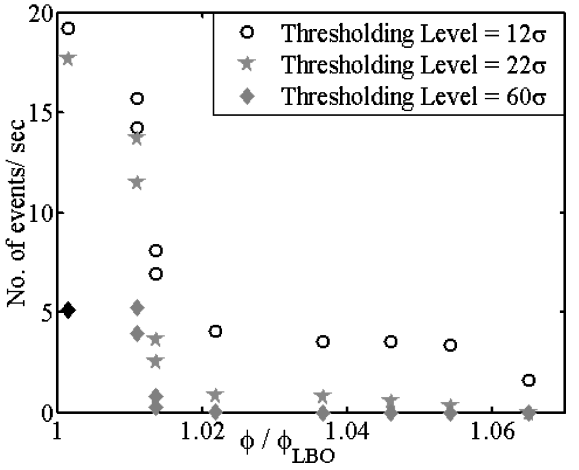

Fig. 13 Dependence of number of events on ϕ/ϕ_{LBO} for three thresholding levels in swirl burner, where σ^2 equals variance of coefficients for stable combustion case, $\phi/\phi_{LBO} = 1.1$.

variance to basis function is minimal for a given ψ. This can be understood when it is noted that the wavelet filtering operation is equivalent to streaming the data through a passband filter. A straightforward application of Parseval's theorem shows that the variance of the filtered data will be quite similar for a variety of different wavelets whose Fourier transforms have similar center frequencies and bandwidths. What then is the advantage of the identification of a customized wavelet? As we suggest in the next section, the key advantage lies in the ability of the customized wavelet to accentuate the amplitude of time-localized events whose shape resembles that of the wavelet. As such, the choice of wavelet impacts the statistics of the filtered signal outliers (time-localized events) whose presence we are interested in detecting. Therefore, the key advantage in customized wavelets lies in their use in conjunction with a discrete event detection algorithm, such as level crossing approaches (discussed in the next section), as opposed to a time-integrated detection algorithm, such as a variance calculation. Similar results were observed in the bluff-body burner.

D. Statistical Approaches

The third- and higher-order statistical moments M_n of the acoustic signal were chosen for analysis because of their sensitivity to outlying or intermittent events. Particular focus was given to M_4, the kurtosis of the acoustic data, which increases slightly ($\sim$30%) for the three burners as they are brought to blowout. This low sensitivity is because the M_4 value is an average estimate of the entire data record. As shown in the next section, a short time-window moving average kurtosis estimate coupled with a thresholding technique is substantially more sensitive.

E. Thresholding Approaches

Thresholding the data provides a convenient way of converting a data stream into a quantitative blowout indicator; for example, a blowout avoidance logic can be invoked when the data exceed a threshold level. As discussed earlier, it is particularly useful for the swirl and bluff-body stabilized flames, which exhibit an increasing number of time-localized events as blowout is approached.

With attention paid first to the swirl burner, the effect of threshold level on level crossing frequency can be understood from Fig. 11, the probability density function (PDF) of the $W_2(t)$ wavelet coefficients for $\phi/\phi_{LBO} = 1.1$, 1.02, and 1.01. The increased presence of high-amplitude outliers close to blowout results in the long tail in the PDF. Figure 11 indicates that the signal from the stable flames rarely exceeds $\sim 30\sigma$, where σ^2 denotes the variance of the $W_2(t)$ coefficients for the stable combustion case $\phi/\phi_{LBO} = 1.1$. Figure 12 shows the dependence of 60σ level crossing frequency (number of crossings per second) and duration (time the signal exceeds the threshold/total time) on ϕ/ϕ_{LBO}. This threshold level is shown by the dashed lines in Fig. 10. The number and duration of events rises from identically zero to about five events/s and 150 ms/s, respectively, just before blowout, as seen in Fig. 12. The effect of threshold level is shown in Fig. 13, the dependence of the number of events on ϕ/ϕ_{LBO} at threshold levels of 12σ, 22σ, and 60σ. Note the two influences of the threshold level: the number of events detected and the ϕ/ϕ_{LBO} value where events are first detected. At lower threshold levels, more events are detected. Furthermore, events are detected at higher ϕ/ϕ_{LBO} values. This was alluded to in Sec. V.A in the discussion of Fig. 6. The tradeoffs in the choice of an optimal threshold level are further illustrated in Fig. 14. The left and right y axes plot the maximum number of events observed before blowout

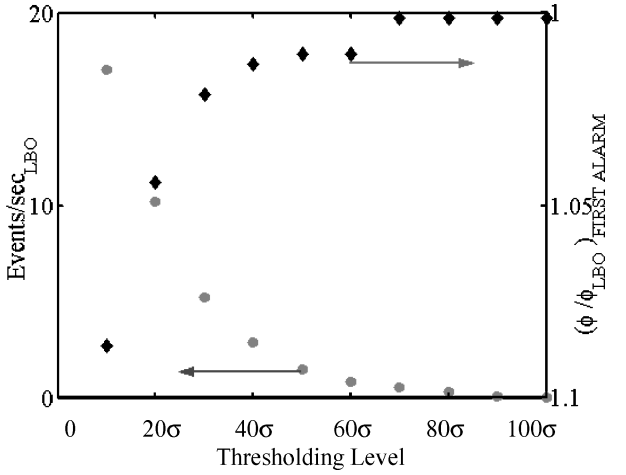

Fig. 14 Variation: ○, in the number of events near blowout and the ϕ value where, ♦, an event is first observed, on thresholding level in swirl burner.

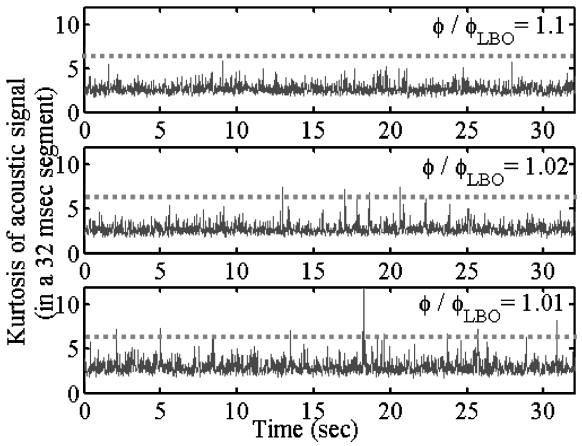

Fig. 15 Time variation of 32 ms moving average kurtosis estimate from swirl burner for ϕ/ϕ_{LBO} = 1.1, 1.02, and 1.01.

(a measure of sensitivity) and the normalized ϕ value where an event is first observed, respectively. As might be anticipated, higher sensitivity results in more alarms at ϕ values where the flame is still reasonably stable.

As discussed earlier, the choice of the wavelet basis function has little influence on the variance of the filtered signal but a larger impact on the level crossing frequency. The event count of the customized wavelet, $W_2(t)$, was found to be almost double that of $W_1(t)$. This indicates that the sensitivity of the thresholding approach may be enhanced by a judicious choice of wavelet.

Analogous results were observed for the bluff-body flame, where comparable number of events per second to that of the swirl burner was observed. However, the average duration of an event is much smaller for the swirl burner (for a given threshold). This shows that the partial extinction/reignition events in the bluff-body burner are of shorter duration than the swirling flame

Thresholding is also useful in conjunction with the moving average calculations of statistical moments of acoustic signal. The temporal dependence of a 32-ms moving average estimate of the kurtosis of the acoustic data from the swirl burner is shown in Fig. 15 at $\phi/\phi_{LBO} = 1.1$, 1.02, and 1.01. The increased presence of large spikes in the kurtosis estimate is observed as blowout is approached. By the application of thresholding techniques similar to these data, results comparable to those shown in Figs. 12–14 were observed here as well.

VI. Conclusions

This paper describes an experimental study of the acoustic characteristics of premixed flames under near blowout conditions. Combustion noise dominates the low-frequency acoustic spectra for all three burners. This regime was found to exhibit a strong dependence on the heat release rates and the degree of flame stabilization. We found a significant increase in intermittent events and/or low-frequency acoustic emission as the flame approached blowout in each of the three burners. The enhanced low-frequency activity in the piloted burner is likely due to large-scale, periodic, flame undulations close to blowout. In the swirl combustor, the bursts in the acoustic signal apparently coincide with short, often spatially localized reignition events. These events increase in frequency and duration as the combustor approaches blowout. The enhanced low-frequency regime appears to be controlled by the time interval between events and the duration of the events. In the bluff-body burner, the flame was asymmetric and similarly unsteady near blowout. Periodic detachment and reattachment of the flame to the flameholder was observed, which manifested itself as low-frequency acoustic emissions.

Based on the preceding observations, spectral-, statistical-, wavelet-, and thresholding-based approaches were used to detect precursors to blowout. The spectral approaches were most sensitive for the swirl burner (∼60) compared to that of piloted burner (∼7) and the bluff-body burner (∼3). The thresholding techniques were found to be most useful when performed after preprocessing of the acoustic data, such as a wavelet filter or moving average calculation of a higher-order statistical moment. Typical values of 5–7 events per second were observed in the swirl and bluff-body burners. These values can be compared with the CO measurements, which increased by factors of two and five for the pilot and swirl burners, respectively.

Acknowledgments

This research was supported by the National Science Foundation under Contract CTS-0092535 (Farley Fisher, Technical Monitor), NASA Ames Research Center under Contract NAG 2-1488 (L. S. Fletcher, Technical Monitor), and the U.S. Department of Energy, Office of Fossil Energy, National Energy Technology Laboratory, under Contract 02-01-SR102 (Richard Wenglarz, Technical Monitor). Chemiluminescence data reported here were obtained by Jerry Seitzman and T. M. Muruganandam.

References

[1]Rosfjord, T. J., and Cohen, J. M., "Evaluation of the Transient Operation of Advanced Gas Turbine Combustors," *Journal of Propulsion and Power*, Vol. 11, No. 3, 1995, pp. 497–504.

[2]DuBell, T. L., and Cifone, A. J., "Combustor Influence on Fighter Engine Operability," AGARD Meeting on Mechanisms of Instability in Liquid Fueled Combustors, 1989.

[3]Barnes, J. C., and Mellor, A. M., "Effects of Unmixedness in Piloted-Lean Premixed Gas Turbine Combustors," *Journal of Propulsion and Power*, Vol. 14, No. 6, pp. 967–973.

[4]Ducruix, S., Schuller, T., Durox, D., and Candel, S. M., "Combustion Dynamics and Instabilities: Elementary Coupling and Driving Mechanisms," *Journal of Propulsion and Power*, Vol. 19, No. 5, 2003, pp. 772–734.

[5]Straub, D. L., and Richards, G. A., "Effect of Fuel Nozzle Configuration on Premix Combustion Dynamics," American Society of Mechanical Engineers, ASME Paper 98-GT-492, June 1998.

[6]Sturgess, G. J., Sloan, D. G., Lesmerises, A. L., Heneghan, S. P., and Ballal, D. R., "Design and Development of a Research Combustor for Lean Blowout Studies," *Journal of Engineering for Gas Turbines and Power*, Vol. 114, No. 1, 1992, pp. 13–19.

[7]Nicholson, H., and Field, J., "Some Experimental Techniques for the Investigation of the Mechanism of Flame Stabilization in the Wake of Bluff Bodies," *Proceedings of the Combustion Institute*, Vol. 3, 1951, pp. 44–68.

[8]Chao, Y. C., Chang, Y. L., Wu, C. Y., and Cheng, T. S., "An Experimental Investigation of the Blowout Process of a Jet Flame," *Proceedings of the Combustion Institute*, Vol. 28, 2000, pp. 335–342.

[9]Longwell, J. P., Chenevey, J., Clark, W., and Frost, E., "Flame Stabilization by Baffles in a High Velocity Gas Stream," *Proceedings of the Combustion Institute*, Vol. 3, 1951, pp. 40–44.

[10]Jensen, W. P., and Shipman, C. W., "Stabilization of Flames in High Speed Flows by Pilot Flames," *Proceedings of the Combustion Institute*, Vol. 7, 1951, pp. 674–680.

[11]Williams, G. C., and Shipman, C. W., "Some Properties of Rod Stabilized Flames of Homogeneous Gas Mixtures," *Proceedings of the Combustion Institute*, Vol. 4, 1953, pp. 733–742.

[12]Lefebvre, A. H., *Gas Turbine Combustion*, Taylor and Francis, Philadelphia, 1998.

[13]Hertzberg, J. R., Shepherd, I. G., and Talbot, L., "Vortex Shedding Behind Rod Stabilized Flames," *Combustion and Flame*, Vol. 86, No. 1, 1991, pp. 1–11.

[14]Ateshkadi, A., McDonnell, V. G., and Samuelson, G. S., "Lean Blowout for a Spray Fired Swirl Stabilized Combustor," *Proceedings of the Combustion Institute*, Vol. 28, 2000, pp. 1281–1288.

[15]Strahle, W., "On Combustion Generated Noise," *Journal of Fluid Mechanics*, Vol. 49, No. 2, 1971, pp. 399–414.

[16]Kotake, S., and Takamoto, K., "Combustion Noise: Effects of the Velocity Turbulence of Unburned Mixture," *Journal of Sound and Vibration*, Vol. 139, No. 1, 1990, pp. 9–20.

[17]Gupta, A. K., Lilley, D. G., and Syred, N., *Swirl Flows*, Abacus, Kent, England, U.K., 1984.

[18]Muruganandam, T. M., Nair, S., Neumeier, Y., Lieuwen, T., and Seitzman, J. M., "Optical and Acoustic Sensing of Lean Blowout Precursors," AIAA Paper 2002-3732, 2002.

[19]Soteriou, M. C., and Mehta, P. G., "Combustion Heat Release Effects on the Dynamics of Bluff Body Stabilized Premixed Reacting Flows," AIAA Paper 2003-0835, 2003.

[20]Groechnig, K., *Foundations of Time-Frequency Analysis*, Birkhaeuser, Boston, 2000.